DOI: 10.1002/anie.200900083

Nanoparticle Crystallinity

# Quantitative Assessment of Nanoparticle Single Crystallinity: Palladium-Catalyzed Splitting of Polycrystalline Metal Oxide Nanoparticles**

*Hyunjin Kim, Myounghoon Lee, Youngki Kim, Jiyoung Huh, Heonjo Kim, Minsik Kim, Taekhoon Kim, Vu Ngoc Phan, Young-Boo Lee, Gi-Ra Yi, Seungjoo Haam, and Kwangyeol Lee**

*Dedicated to Prof. Joon T. Park on the occasion of his 60th birthday*

Magnetic metal oxide nanoparticles are among the most studied nanoparticle systems because of various potential applications in magnetic resonance imaging (MRI),[1] magnetic bioseparation,[2] and other procedures.[3] A number of synthetic methods have been developed for high-quality metal oxide nanoparticles,[4] each with high single crystallinity and size monodispersity. Quality control of nanoparticles would be crucial for future usage, with increasingly more nanoparticle systems finding their way into nanomedicines. The single crystallinity of magnetic nanoparticles, in particular, served as a guide for material quality because the magnetic property of nanoparticles is closely related to the magnetic domain size. However, the assessment of nanoparticle single crystallinity has been, thus far, at best qualitative, because it is practically impossible to examine all the nanoparticles on the grid of the microscope in transmission electron microscopy (TEM), not to mention all those formed within a reaction batch. Thus, it is necessary to develop a simple method for a statistically meaningful, quantitative assessment of the single crystallinity of nanoparticles. Herein, we report a simple, definitive method to provide a visual indication of the presence of nanoparticle polycrystallinity.

[*] H. Kim, M. Lee, Y. Kim, J. Huh, H. Kim, M. Kim, T. Kim, V. N. Phan, Prof. K. Lee
Department of Chemistry, Korea University, Seoul 136-701 (Korea)
Fax: (+82) 2-3290-3121
E-mail: kylee1@korea.ac.kr
Dr. Y.-B. Lee
Korea Basic Research Institute (KBSI), JeonJu 561-756 (Korea)
Dr. G.-R. Yi
Nano–Bio System Research Team, KBSI, Seoul 136-713 (Korea)
Prof. S. Haam
Department of Chemical & Biomolecular Engineering
Yonsei University, Seoul 120-749 (Korea)

[**] This work was supported by MOST (KOSEF M10755020001-08N5502-00110), KRF-2008-314-C00234, MIHWAF (the Korea Health 21 R&D Project: A085136), and the Future Key Technology Program of KIST. We thank the staff of KBSI at Chuncheon for technical assistance in the TEM analyses. We also thank Prof. Paras N. Prasad at SUNY-Buffalo for in-depth discussions about manuscript preparation.

Supporting information for this article is available on the WWW under http://dx.doi.org/10.1002/anie.200900083.

We discovered that the nanocrystalline $Fe_3O_4$ phase slowly disintegrates over 24 h to give soluble, air-sensitive iron complexes, which are characterized by mass spectrometry (Supporting Information, Figure S1) in the solvent system oleylamine/trioctylphosphine (OA/TOP, 1:9, v/v) at high temperature (300 °C). Interestingly, $Fe_3O_4$ phase disintegration is greatly suppressed at a low content of TOP; even after 24 h at 300 °C in OA/TOP (9:1, v/v), the diameters of $Fe_3O_4$ nanoparticles are little changed (Supporting Information, Figure S2). By introducing catalytic Pd in the form of $[Pd(acac)_2]$ (acac = acetylacetonate), however, we could greatly accelerate the etching of $Fe_3O_4$ even in a low-TOP medium (OA/TOP 9:1, v/v), in which the $Fe_3O_4$ phase would otherwise be stable. Most notably, the Pd-assisted $Fe_3O_4$ phase disintegration was fastest for the interfaces separating single-crystalline domains within a bicrystalline $Fe_3O_4$ nanoparticle. By simply counting split nanoparticles in the TEM image, quantitative assessment of nanoparticle single crystallinity can be accomplished.

Modification of the reported $Fe_3O_4$ synthesis[4a] (see synthetic details and Figure S3 in the Supporting Information) gives $Fe_3O_4$ bicrystals as the major product. The bicrystalline nature of a selected $Fe_3O_4$ nanoparticle is demonstrated by its high-resolution TEM (HRTEM) image (Figure 1c). Heating the OA/TOP (9:1, v/v) solution of bicrystalline $Fe_3O_4$ nanoparticles at 300 °C for 1.5 h under a $N_2$ blanket in the presence of a catalytic amount of $[Pd(acac)_2]$ resulted in nearly 60% of nanoparticles split in the middle, as shown in Figure 1b. It can be stated that at least 60% of the nanoparticles shown in Figure 1a are not single-crystalline, which is the first quantitative assessment of nanoparticle single crystallinity. Because the observation of split nanoparticles from only one direction would undoubtedly lead to undercounting of these particles, we examined nanoparticles of the same reaction batch by tilting the supporting TEM grid at various angles. The hemispherical nature of the split nanoparticles, which resulted from the removal of a $Fe_3O_4$ disc that was approximately 2 nm thick and contained a crystal-domain interface from a $Fe_3O_4$ bicrystal, can be clearly demonstrated (Supporting Information, Figure S4). Certain nanoparticles seem to be intact at first glance, but they readily reveal the chasm in the structure at appropriate observation angles to show again that around 60% of the nanoparticles are not single-crystalline, as found above. Thus, the TEM grid

  

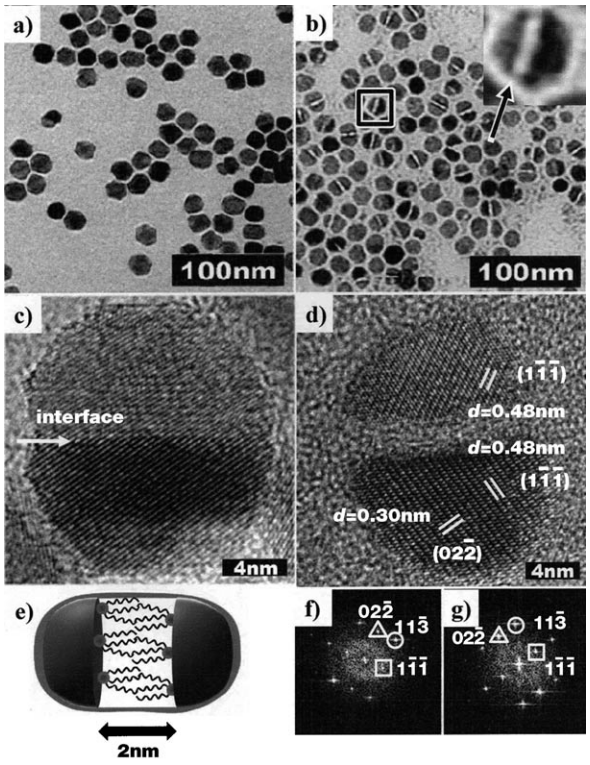


***Figure 1.*** TEM images of a) bicrystalline $Fe_3O_4$ nanoparticles and b) split hemispherical nanoparticles linked by a thin amorphous layer. The presence of a thin layer is indicated by an arrow in the inset of (b). HRTEM images of c) a bicrystalline iron oxide nanoparticle in (a) with the crystal-domain interface clearly shown and d) the split nanoparticle shown in (b). e) Schematic diagram of the cleaved nanoparticle shown in (d). f,g) Fast Fourier transform images along the ⟨211⟩ zone axis for the f) upper and g) lower hemispherical nanoparticles in (d).

should be observed from various directions to determine the precise percentage of split nanoparticles.

Clearly, the interface between single-crystalline domains of a bicrystalline nanoparticle is very unstable, because it is etched out at a speed unmatched by other surfactant-coated crystal planes. The planar defect at the crystal-domain interface seems to be responsible for the high instability. It was recently demonstrated that etching of certain crystal planes in a given metal nanoparticle can be facilitated over other crystal planes.[5] However, the degree of disparity in crystal-plane reactivities observed in this study is unprecedented for both metal and metal oxide systems. Interestingly, all split $Fe_3O_4$ nanocrystals invariably contain a gap of approximately 2 nm in the middle and the split nanoparticles are joined by a thin, amorphous layer (Figure 1b, inset; see also Figure S5 in the Supporting Information for further HRTEM images showing the presence of amorphous thin layers connecting the split hemispherical nanoparticles). This finding implies that the accelerated etching at the interface should slow down when the separation between two hemispheres is approximately 2 nm, which is large enough to allow strong protection against further etching by standing TOP surfactants on the two inner $Fe_3O_4$ surfaces, newly created by etching.

To further understand the Pd-assisted etching process of $Fe_3O_4$ and the formation of an amorphous thin layer connecting split nanoparticles, we tested the method developed above for spherical $(12 \pm 0.7)$ nm $Fe_3O_4$ nanoparticles[4b] with a high single crystallinity (see Figure S6 in the Supporting Information, which shows temporal TEM images for etching of spherical iron oxide nanoparticles). Most notably, no splitting of iron oxide nanoparticles was observed for this nanoparticle system and only hollow spheres, occasionally with small dots in the center, and wormlike nanoparticles resulted. The hollow spheres and wormlike particles formed do not exhibit any crystallinity, while the presence of iron, phosphorus, and oxygen in the material is revealed by energy-dispersive X-ray analysis (Supporting Information, Figure S7).

Unchanged iron oxide nanoparticles are observed even after 9 h of Pd-assisted etching reaction, which suggests a high single crystallinity for the whole nanoparticle sample; splitting of nanoparticles was very fast and was finished within 1.5 h for polycrystalline iron oxide nanoparticles. By comparing the sizes of the original nanoparticles and resulting hollow spheres, it is evident that $Fe_3O_4$ nanoparticles acted as both the template and the precursor. It is likely that during the initial reaction stage, the decomposed products of $Fe_3O_4$ are rapidly converted into a thin (ca. 2 nm) amorphous and porous layer on the $Fe_3O_4$ nanoparticle surface. At a later stage, however, the soluble iron species might diffuse out through the porous layer, without further thickening the layer, because the interior surface of the amorphous hollow sphere would be effectively protected by coordinated surfactants. The soluble iron species, not confined within the hollow sphere, might be subsequently decomposed to form small wormlike particles in the solution. The formation of hollow spheres from inorganic nanoparticles could be explained by the Kirkendall effect.[6] In our case, the conversion of $Fe_3O_4$ into soluble species by a Pd catalytic system drives the outward diffusion of iron atoms to form a hollow structure.

No reaction was observed in the absence of OA, thus indicating its crucial role in activating the Pd catalytic system. Under the reaction conditions used, $[Pd(acac)_2]$ decomposes to form Pd nanoparticles of approximately 2 nm (Supporting Information, Figure S8). It has previously been shown that $Pd^{II}$ can be reduced to $Pd^0$ at elevated temperatures in the presence of OA.[7] The role of OA as a reducing agent has also been demonstrated in the conversion of CoO into the Co phase.[8] The formation of amorphous spheres by etching of $Fe_3O_4$ nanoparticles requires the easy access of catalysts through the porous amorphous layer. Pd nanoparticles that are approximately 2 nm in diameter are certainly not capable of such permeability. It has been demonstrated in other Pd nanoparticle systems that catalytic $Pd^0$ species can be leached from the Pd nanoparticles.[9] Thus, the small, soluble Pd species leached from Pd nanoparticles, which can easily enter the porous amorphous layer on the $Fe_3O_4$ nanoparticle, seem to be the actual catalysts capable of destabilizing the $Fe_3O_4$ phase. This could be further corroborated by the fact that hollow spheres can also be obtained from etching of $Fe_3O_4$ nanoparticles, even if much larger Pd nanoparticles ($> 5$ nm)

  

are used as catalysts instead of [Pd(acac)$_2$] (Supporting Information, Figure S9).

It is well known that Pd$^0$ species can catalyze the oxidation reaction of phosphines.[10] We found that Pd catalyst, most likely in the form of soluble Pd$^0$ species, facilitates the oxidation of TOP to form trioctylphosphine oxide (TOPO) in the presence of trace amounts of oxygen, whereas the formation of TOPO is greatly retarded by the presence of OA alone (Supporting Information, Figure S10). The TOPO formed in situ, however, does not seem to be the actual etchant for the $Fe_3O_4$ phase; no reaction was observed for $Fe_3O_4$ nanoparticles (25 mg) in an OA/TOP/TOPO (9 mL/0.2 mL/0.7 g) mixture at 300 °C. It is also known that $H_2$ can be produced from the dehydrogenation of amines in the presence of Pd catalyst.[11] Thus, the $Fe_3O_4$/OA/TOP/TOPO (25 mg/9 mL/0.9 mL/0.1 g; small amount of TOPO added to mimic the Pd catalyst effect) mixture was heated at 300 °C under 10% $H_2/N_2$. Again no reaction was observed; the presence of $H_2$ is not crucial for the destabilization of the $Fe_3O_4$ phase. Thus, it seems that the role of OA is confined to the reduction of Pd$^{II}$ ions to Pd nanoparticles or soluble Pd$^0$ species. In summary, OA reduces Pd$^{II}$ ions to form soluble Pd$^0$ species and Pd nanoparticles. The soluble Pd$^0$ species, formed directly from Pd$^{II}$ species or leached from Pd nanoparticles, might catalyze the transformation of coordinated TOP into TOPO by using the oxygen atoms in $Fe_3O_4$ as the oxygen source, because $Fe_3O_4$ is the readily available source of oxygen in the reaction mixture. Concomitantly, Fe atoms stabilized by TOP, TOPO, and OA ligands might be detached from the $Fe_3O_4$ nanoparticle. However, more study is needed to fully understand this Pd-assisted destabilization of the $Fe_3O_4$ phase.

Further insight into the etching process came from etching other types of single-crystalline iron oxide nanoparticles, namely, slightly larger (13.2 ± 0.8) nm spherical $Fe_3O_4$ nanoparticles,[4b] (16.5 ± 2.0) nm $Fe_3O_4$ nanocubes,[12] and (17.6 ± 2.0) nm Fe@$Fe_3O_4$ nanocubes[13] to form double concentric hollow spheres, double concentric hollow nanoboxes, and single nanoboxes, respectively (Supporting Information, Figure S11). The spherical and cubelike morphologies are sustained in the final products, thus indicating the very fast formation of a thin amorphous layer on the surface of the nanostructure at an early stage. The presence of a small hollow sphere or nanobox within a large hollow sphere or nanobox, respectively, indicates that a smaller $Fe_3O_4$ nanocrystal formed by etching inside a hollow sphere can also act as a template for another amorphous layer. Closer examination of these unprecedented double hollow nanostructures shows a gap distance of approximately 2 nm between concentric hollow structures, which corresponds to roughly twice the height of a standing TOP surfactant as in the split $Fe_3O_4$ nanoparticles of Figure 1b. Thus, the inner surface of an amorphous hollow sphere seems to be effectively coordinated by a layer of TOP surfactant.

Furthermore, the etching of the $Fe_3O_4$ phase proceeds rapidly until a robust bilayer of surfactants (one layer on the inner wall of an amorphous hollow sphere and the other layer on the trapped $Fe_3O_4$ nanocrystal surface) can form and effectively block the passage of escaping soluble iron species, which would then be converted to another amorphous layer on the trapped $Fe_3O_4$ nanocrystal. If the interior volume of a hollow sphere is not large enough to contain a concentric bilayer of surfactants, then the formation of an inner hollow sphere is not possible. This also explains why the smaller hollow spheres in Figure S6 (Supporting Information) contain only a small dot, not a complete hollow sphere, in the center of a hollow sphere, or are even empty. Interestingly, the etching of Fe@$Fe_3O_4$ nanoparticles results in the formation of single hollow nanoboxes. Clearly, the Fe nanoparticle core is so quickly removed that it cannot serve as a template for an amorphous layer, which corroborates the proposed reaction mechanism involving the removal of oxygen atoms from iron atoms.

The disparate etching behaviors of polycrystalline and single-crystalline $Fe_3O_4$ nanocrystals are depicted in Figure 2.

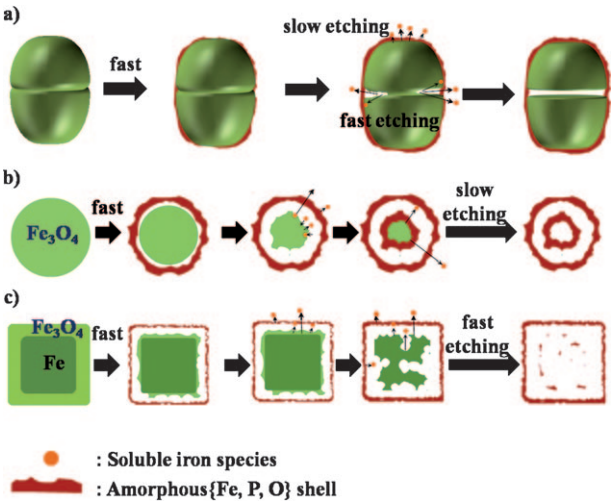


***Figure 2.*** Etching processes to form a) two hemispherical nanoparticles trapped within an amorphous hollow sphere from a bicrystalline $Fe_3O_4$ nanoparticle, b) a concentric double hollow sphere from a $Fe_3O_4$ nanoparticle, and c) a single nanobox from a Fe@$Fe_3O_4$ nanocube.

Obviously, the time required to form a thin amorphous layer on the surface of $Fe_3O_4$ nanoparticle is comparable to or slightly shorter than the time (1.5 h) required to remove the entire $Fe_3O_4$ disc that was approximately 2 nm thick and contained the crystal-domain interface of a polycrystalline $Fe_3O_4$ nanocrystal (Figure 2a); without prior formation of the porous, amorphous layer on $Fe_3O_4$, the split hemispherical nanoparticles would fall apart. Figure 2b,c depicts the proposed pathways for the formation of hollow structures with amorphous walls. The same amorphous wall provided a structural support for the split hemispherical nanoparticles to be joined together as in Figure 1b. Although the formation of concentric double hollow spheres or nanoboxes from $Fe_3O_4$ nanoparticles or $Fe_3O_4$ nanocubes, respectively, requires at least 20 h for completion, the formation of nanoboxes from Fe@$Fe_3O_4$ nanocubes requires only 7 h. Furthermore, the long time required to completely decompose single-crystalline $Fe_3O_4$ or Fe@$Fe_3O_4$ nanoparticles suggests a high degree of $Fe_3O_4$ nanoparticle surface stabilization by coordinated

  

surfactants. Without a high-energy crystal-domain interface, the outer surfaces of these single-crystalline nanoparticles seem to be rather evenly protected by surfactants, which results in isotropic etching of the nanoparticles.

Etching of a core–shell-structured Pd@$Fe_3O_4$ nanoparticle, prepared by modification of Au@$Fe_3O_4$ synthesis,[14] would always seek and reveal a Pd nanoparticle, because Pd@$Fe_3O_4$ nanoparticles would undoubtedly have a polycrystallinity initiating from the heterogeneous Pd nanoparticle. The different crystal-growth directions are clearly demonstrated by the HRTEM images shown in Figure 3c. Even

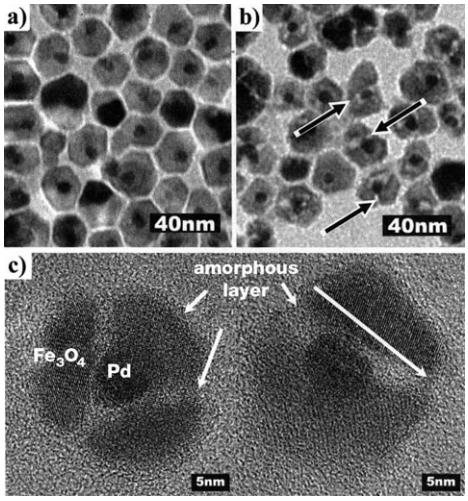


***Figure 3.*** TEM images of a) Pd@$Fe_3O_4$ core–shell nanoparticles, b) flowerlike Pd@$Fe_3O_4$ nanoparticles obtained by etching the particles in (a) (arrows indicate interfaces), and c) HRTEM images of flowerlike nanoparticles with etched out crystal-domain interfaces. The images are slightly out of focus to show the presence of an amorphous layer.

when a large, well-faceted $Fe_3O_4$ polyhedron shell encapsulates a Pd core, the presence of polycrystallinity in the $Fe_3O_4$ phase is revealed at appropriate grid-tilt angles (Supporting Information, Figure S14). Since the catalytic Pd nanoparticle is now exposed to the outside through the chasm of magnetic $Fe_3O_4$ grains, the Pd@$\{Fe_3O_4\}_n$ flowerlike structure might be used as a magnetically separable catalyst after removal of the protective amorphous layer.

To show the utility of the developed etching method in testing the degree of single crystallinity of $Fe_3O_4$ nanoparticles, we prepared $Fe_3O_4$ nanoparticle mixtures with varying degrees of single-crystalline nanoparticles in their compositions and performed the etching experiment on these samples. As expected, the quantitative nature of the etching methodology for checking single crystallinity was well demonstrated (Supporting Information, Figure S15).

The above-mentioned method to discern the single crystallinity of iron oxide nanoparticles was further tested for other nanoparticle systems, potentially useful for MRI, with the compositions $Fe_2O_3$, $MnFe_2O_4$, $CoFe_2O_4$, and MnO, each prepared by modification of reported methods (see the Supporting Information for synthetic details) to increase the fraction of nanoparticles with polycrystallinity within a reaction batch. These nanoparticles, as intended, do not exhibit a high single crystallinity, as judged from the salient presence of a significant number of split nanocrystals in their TEM images (Figure 4). The single-crystalline counterparts of

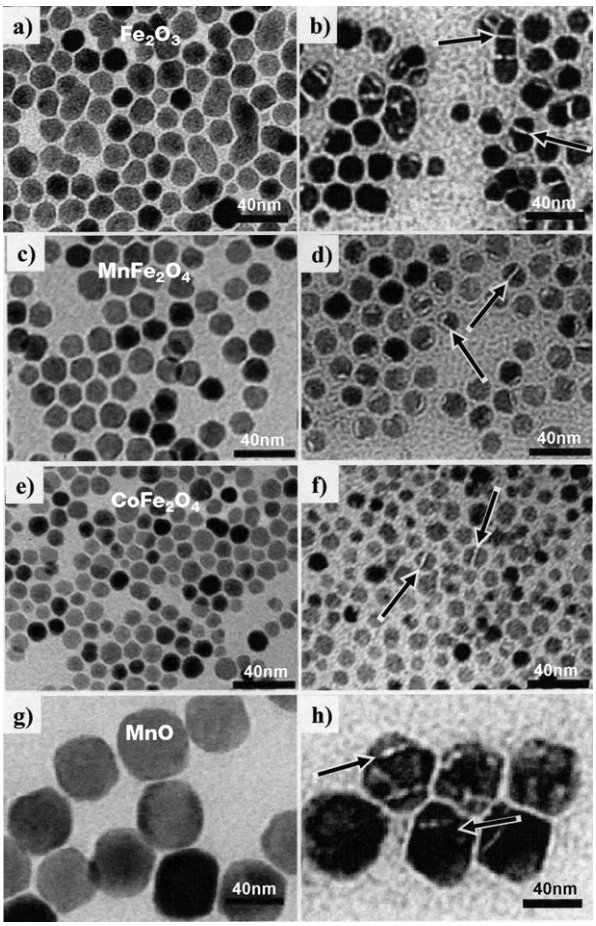


***Figure 4.*** TEM images of polycrystalline nanoparticles (a,c,e,g) and nanoparticles after etching (b,d,f,h). a,b) $Fe_2O_3$; c,d) $MnFe_2O_4$; e,f) $CoFe_2O_4$; and g,h) MnO. Some of the nanoparticle crystal-domain interfaces in the polycrystalline nanoparticles are indicated by arrows.

these metal oxide systems[15] are very robust under the same reaction conditions (Supporting Information, Figure S16). Clearly, the etching mechanism for $Fe_3O_4$ can also be applied to other metal oxides, namely, $Fe_2O_3$, $MnFe_2O_4$, $CoFe_2O_4$, and MnO. The magnetic behavior, and thus the MRI ability in particular, of the polycrystalline nanoparticles with multiple small single-crystalline domains would deviate significantly from that of ideal, all-single-crystalline nanoparticles.

In summary, we have reported the first Pd-nanoparticle-catalyzed etching of various metal oxide ($Fe_2O_3$, $Fe_3O_4$, $MnFe_2O_4$, $CoFe_2O_4$, and MnO) nanoparticles for the quantitative assessment of nanoparticle single crystallinity. By using the very fast etching speed of the grain interface within bi- or polycrystalline nanocrystals, a simple quantitative method was developed to assess the single crystallinity of metal oxide nanoparticles. We believe our method can provide a strict material quality guideline for metal oxide nanoparticle-based applications. For example, the high single crystallinity of magnetic metal oxide nanoparticles might have to be

  

guaranteed, before they are used in MRI for humans, for a high resolution at minimal nanoparticle dosages. In addition, interesting hollow concentric nanostructures and flowerlike nanostructures, which are otherwise highly difficult to prepare, could also be obtained by the nanoetching method. The catalyst-assisted nanoetching described herein would greatly contribute to the nascent field of post-synthetic structural modification of nanoparticles for novel shape-dependent properties.

Received: January 6, 2009
Revised: March 18, 2009
Published online: June 9, 2009

**Keywords:** crystal growth · magnetic properties · nanoparticles · nanostructures · palladium

[1] a) J.-H. Lee, Y.-M. Huh, Y.-W. Jun, J.-W. Seo, J.-T. Jang, H.-T. Song, S. Kim, E.-J. Cho, H.-G. Yoon, J.-S. Suh, J. Cheon, *Nat. Med.* **2007**, *13*, 95 – 99; b) J. Yang, C.-H. Lee, H.-J. Ko, J.-S. Suh, H.-G. Yoon, K. Lee, Y.-M. Huh, S. Haam, *Angew. Chem.* **2007**, *119*, 8992 – 8995; *Angew. Chem. Int. Ed.* **2007**, *46*, 8836 – 8839; c) Y.-W. Jun, Y.-W. Seo, J. Cheon, *Acc. Chem. Res.* **2008**, *41*, 179 – 189; d) S. A. Corr, S. J. Bryne, R. Tekoriute, C. J. Meledandri, D. F. Brougham, M. Lynch, C. Kerskens, L. O'Dwyer, Y. K. Gun'ko, *J. Am. Chem. Soc.* **2008**, *130*, 4214 – 4215; e) J. Cheon, J.-H. Lee, *Acc. Chem. Res.* **2008**, *41*, 1630 – 1640; f) H. B. Na, J. H. Lee, K. An, Y. I. Park, M. Park, I. S. Lee, D.-H. Nam, S. T. Kim, S.-H. Kim, S.-W. Kim, K.-H Lim, K.-S. Kim, S.-O. Kim, T. Hyeon, *Angew. Chem.* **2007**, *119*, 5493 – 5497; *Angew. Chem. Int. Ed.* **2007**, *46*, 5397 – 5401.

[2] a) C. Xu, K. Xu, H. Gu, R. Zheng, H. Liu, X. Zhang, Z. Guo, B. Xu, *J. Am. Chem. Soc.* **2004**, *126*, 9938 – 9939; b) A. Palani, J.-S. Lee, J. Huh, M. Kim, Y.-J. Lee, J. H. Chang, K. Lee, S.-W. Lee, *J. Proteome Res.* **2008**, *7*, 3591 – 3596; c) H. L. Liu, C. H. Sonn, J. H. Wu, K.-M. Lee, Y. K. Kim, *Biomaterials* **2008**, *29*, 4003 – 4011; d) W.-J. Chen, P.-J. Tsai, Y.-C. Chen, *Small* **2008**, *4*, 485 – 491.

[3] a) C. T. Yavuz, J. T. Mayo, W. W. Yu, A. Prakash, J. C. Falkner, S. Yean, L. Cong, H. J. Shipley, A. Kan, M. Tomson, D. Natelson, V. L. Colvin, *Science* **2006**, *314*, 964 – 967; b) S. Bae, S. W. Lee, Y. Takemura, *Appl. Phys. Lett.* **2006**, *89*, 252503; c) A. M. Derfus, G. von Maltzahn, T. J. Harris, T. Duza, K. S. Vecchio, E. Ruoslahti, S. N. Bhatia, *Adv. Mater.* **2007**, *19*, 3932 – 3936; d) C. Kaittanis, S. A. Naser, J. M. Perez, *Nano Lett.* **2007**, *7*, 380 – 383.

[4] a) S. Sun, H. Zeng, D. B. Robinson, S. Raoux, P. M. Rice, S. X. Wang, G. Li, *J. Am. Chem. Soc.* **2004**, *126*, 273 – 279; b) J. Park, K. An, Y. Hwang, J.-G. Park, H.-J. Noh, J.-Y. Kim, J.-H. Park, N.-M. Hwang, T. Hyeon, *Nat. Mater.* **2004**, *3*, 891 – 895; c) N. Bao, L. Shen, Y. Wang, P. Padhan, A. Gupta, *J. Am. Chem. Soc.* **2007**, *129*, 12374 – 12375; d) M. Niederberger, *Acc. Chem. Res.* **2007**, *40*, 793 – 800.

[5] a) D. Kim, J. Park, K. An, N.-K. Yang, J.-G. Park, T. Hyeon, *J. Am. Chem. Soc.* **2007**, *129*, 5812 – 5813; b) X. Lu, L. Au, J. McLellan, Z.-Y. Li, M. Marquez, Y. Xia, *Nano Lett.* **2007**, *7*, 1764 – 1769.

[6] a) Y. Yin, R. M. Rioux, C. K. Erdonmez, S. Hughes, G. A. Somorjai, A. P. Alivisatos, *Science* **2004**, *304*, 711 – 714; b) K. An, S. G. Kwon, M. Park, H. B. Na, S.-I Baik, J. H. Yu, D. Kim, J. S. Son, Y. W. Kim, I. C. Song, W. K. Moon, H. M. Park, T. Hyeon, *Nano Lett.* **2008**, *8*, 4252 – 4258.

[7] a) S.-W. Kim, J. Park, Y. Jang, Y. Chung, S. Hwang, T. Hyeon, *Nano Lett.* **2003**, *3*, 1289 – 1291; b) A. H. Tian, J.-Y. Kim, J. Y. Shi, K. Kim, K. Lee, *J. Power Sources* **2007**, *167*, 302 – 308.

[8] K. M. Nam, J. H. Shim, H. Ki, S.-I. Choi, G. Lee, J. K. Jang, Y. Jo, M.-H. Jung, H. Song, J. T. Park, *Angew. Chem.* **2008**, *120*, 9646 – 9650; *Angew. Chem. Int. Ed.* **2008**, *47*, 9504 – 9508.

[9] L. Wu, Z.-W. Li, F. Zhang, Y.-M. He, Q.-H. Fan, *Adv. Synth. Catal.* **2008**, *350*, 846 – 862.

[10] V. V. Grushin, *Organometallics* **2001**, *20*, 3950 – 3961.

[11] a) S. Murahashi, N. Yoshimura, T. Tsumiyama, T. Kojima, *J. Am. Chem. Soc.* **1983**, *105*, 5002 – 5011; b) R. B. Wilson, Jr., R. M. Laine, *J. Am. Chem. Soc.* **1985**, *107*, 361 – 369.

[12] M. V. Kovalenko, M. I. Bodnarchuk, R. T. Lechner, G. Hesser, F. Schäffler, W. Heiss, *J. Am. Chem. Soc.* **2007**, *129*, 6352 – 6353.

[13] A. Shavel, B. Rodríguez-González, M. Spasova, M. Farle, L. M. Liz-Marzán, *Adv. Funct. Mater.* **2007**, *17*, 3870 – 3876.

[14] W. Shi, H. Zeng, Y. Sahoo, T. Y. Ohulchanskyy, Y. Ding, Z. L. Wang, M. Swihart, P. N. Prasad, *Nano Lett.* **2006**, *6*, 875 – 881.

[15] a) A. Ahniyaz, Y. Sakamoto, L. Bergström, *Proc. Natl. Acad. Sci. USA* **2007**, *104*, 17570 – 17574; b) N. Bao, L. Shen, Y. Wang, P. Padhan, A. Gupta, *J. Am. Chem. Soc.* **2007**, *129*, 12374 – 12375; c) D. Zitoun, N. Pinna, N. Frolet, C. Belin, *J. Am. Chem. Soc.* **2005**, *127*, 15034 – 15035.

  